ELSEVIER

Contents lists available at ScienceDirect

Chemical Geology

journal homepage: www.elsevier.com/locate/chemgeo





Fate and availability of dust-borne phosphorus in a sub-humid temperate forest

Zhuojun Zhang ^{a,b,f}, Hairuo Mao ^b, Zhi-Qi Zhao ^{c,*}, Shilu Wang ^a, Cong-Qiang Liu ^d, Yongfeng Hu ^e, Mengqiang Zhu ^{b,*}

- a State Key Laboratory of Environmental Geochemistry, Institute of Geochemistry, Chinese Academy of Sciences, Guiyang, Guizhou 550081, China
- b Department of Ecosystem Science and Management, University of Wyoming, Laramie, WY 82071, United States
- ^c School of Earth Science and Resources, Chang'an University, Xi'an, Shaanxi 710054, China
- ^d Institute of Surface-Earth System Sciences, Tianjin University, Tianjin 300072, China
- ^e Canadian Light Source Inc., University of Saskatchewan, Saskatoon, Saskatchewan S7N 2V3, Canada
- f University of Chinese Academy of Sciences, Beijing 100049, China

ARTICLE INFO

Editor: Hailiang Dong

Keywords:
Phosphorus speciation and availability
Aeolian dust inputs
Sub-humid temperate forest
Particle size fractions
X-ray absorption near edge structure
spectroscopy

ABSTRACT

Aeolian dust deposition is an important phosphorus (P) input to terrestrial ecosystems, but it lacks evidence of how dust inputs supply available P and affect P geochemistry and dynamics in soils of sub-humid ecosystems. We determined soil P speciation using P K-edge X-ray absorption near edge spectroscopy and P availability using modified Hedley sequential chemical extractions in a weakly acidic soil profile (2.5 m thick) in a sub-humid temperate forest ecosystem. The soil profile receives substantial dust inputs that account for 34.8% - 53.5% of the soil mass at depths based on a Sr isotope analysis. The acidic topsoils (5 < pH < 5.5) contain Ca-bound P (Ca-P) that accounts for 4%-18% of total soil P. Since Ca-P compounds are unstable and transform to other forms at pH < 5.5, continuous inputs of dust materials rich in Ca-P must occur to sustain the considerable Ca-P in the topsoils. Across all depths, soil Ca-P positively correlates with soil labile Pi (both resin and NaHCO3 extracted) in proportion, suggesting that dissolution of dust-borne Ca-P compounds replenishes the labile Pi pool. On the other hand, weathering of the Fe-rich dusts leads to formation of abundant iron oxides that in turn favors formation of occluded P (44-85%) and Fe (and Al)-bound P (57-83%), which may fix released P from the dust-borne Ca-P dissolution and reduce soil P availability in a long term. Interestingly, the saprolite layer has an unexpectedly high weathering degree with nearly depleted Ca-P, likely caused by dust inputs that increase soil moisture and microbial activities and accordingly weathering. Our study identifies that continuous deposition and subsequent dissolution of dust-borne Ca-P compounds in acidic soils sustain soil P availability. The study also highlights that aeolian dust inputs affect soil P availability and dynamics in a sub-humid forest ecosystem not only by acting as a bioavailable P source but also altering soil chemistry and weathering.

1. Introduction

Phosphorus (P) is an essential nutrient and its bioavailability controls critical functions and properties of terrestrial ecosystems (Elser et al., 2007; Filippelli, 2008; Föllmi, 1996; Tyrrell, 1999). Aeolian mineral dust is an important P source to terrestrial ecosystems (Aciego et al., 2017; Chadwick et al., 1999; Okin et al., 2004; Pett-Ridge, 2009; Porder et al., 2007). Mineral dust inputs can replenish P stock of ecosystems, such as for tropical rainforests highly limited by P (Chadwick et al., 1999; Eger et al., 2013; Kurtz et al., 2001; Okin et al., 2004; Pett-Ridge, 2009; Richardson et al., 2004; Yu et al., 2015) and semi-arid

ecosystems that are located at the margins of dust source areas and thus receive large quantities of dust inputs (Selmants and Hart, 2008). Dust inputs to supply P to ecosystems may become more important in the context of global environmental change since dust production is predicted to increase as land-use intensifies and droughts become more severe and frequent due to global warming (Dai, 2013; Neff et al., 2008).

Pedogenic processes, including weathering, leaching, vertical translocation, and biological cycling, determine the fate and availability of dust-borne P in a dust-receiving ecosystem, and the relative importance of these processes depends on the climate of the ecosystem (Zhang et al., 2021). Apatite and other calcium-bound P (Ca-P) species are often

E-mail addresses: zhaozhiqi@chd.edu.cn (Z.-Q. Zhao), mzhu6@uwyo.edu (M. Zhu).

^{*} Corresponding authors.

the dominant P compounds in mineral dust while Fe- and Al-bound P [(Fe + Al)-P] and organic P (Po) can be significant as well (Gu et al., 2019; Hudson-Edwards et al., 2014; Longo et al., 2014; Zhang et al., 2018) although long-distance traveled mineral dust could contain dominant (Fe + Al)-P due to atmospheric acidification and particle sorting (Dam et al., 2021). In humid and super-humid ecosystems, Ca-P compounds in mineral dust are readily dissolved in the acidic, organicrich surface layer of forest grounds (Crews et al., 1995; Eger et al., 2013; Vogel et al., 2021). The released P can be quickly absorbed by organisms to form Po in the surface organic horizon where the plant roots and microbial P cycling are concentrated in the super-humid climate (Eger et al., 2013), or leach down to increase the level of non-occluded P in topsoils of tropical rainforests (Crews et al., 1995). In contrast, mineral dust slowly releases P to alkaline and circumneutral soils characteristic of semi-arid and seasonally dry environments due to water limitation and thus weak weathering, leading to accumulation of dust-borne Ca-P in soils (Gallardo et al., 2020; Gu et al., 2019). Compared to humid, super-humid, arid and semi-arid ecosystems, the fate and availability of dust-borne P remains less understood in sub-humid ecosystems that cover about 10% of Earth's land surface (Prăvălie, 2016) and are expected to increase during the twenty-first century due to forecasted increasing aridity (Huang et al., 2016; Sauchyn et al., 2002). We hypothesize that dust-borne P has different fate and availability traits in a sub-humid ecosystem compared to others because both the dust inputs and water availability are at moderate levels compared to humid (high water availability but low dust inputs) and semi-arid (low water availability but high dust inputs) ecosystems.

In this study, we aim to determine the fate and availability of dustborne P and how dust inputs affect soil P geochemistry and dynamics in a sub-humid ecosystem. We quantified soil mass contributions of dust inputs and determined P distribution, speciation, and availability in a soil profile of a sub-humid temperate forest ecosystem located in the margin of dust source areas. Sequential chemical extractions and P K-edge X-ray near edge structure absorption (XANES) spectroscopy were used to characterize P availability and speciation, respectively. The soils were also separated into different size fractions, corresponding to varying weathering degrees, to further evaluate the influence of dust inputs on soil P speciation. We also conducted a dust acidification test to infer how susceptible dust-borne Ca-P compounds are to dissolution in acidic soils.

2. Materials and methods

2.1. Study site and soil sampling

The study site was located in Dunhua city, Jilin, China in a subhumid mid-temperate climate zone. The site had a mean annual temperature of 2.6 $^{\circ}$ C and a mean annual precipitation of 598 mm. The site was covered by a broadleaved forest. The exposed rock in the study site was Indosinian granite. The site received the aeolian dust inputs that were mainly originated from the loess and desert in the northern China because it was in the northeastern margin of the deserts and Loess Plateau in the northern China (Hoffmann et al., 2008; Ma et al., 2013; Shao and Dong, 2006; Sun, 2002) (Fig. 1a). The soil profiles had a gentle slope ($<3^{\circ}$), which favored dust accumulation and stabilization.

Two soil profiles were sampled from the study site. Preliminary analyses showed that these two profiles had similar concentrations of major elements and Sr isotopic composition (Fig. S1). However, due to a

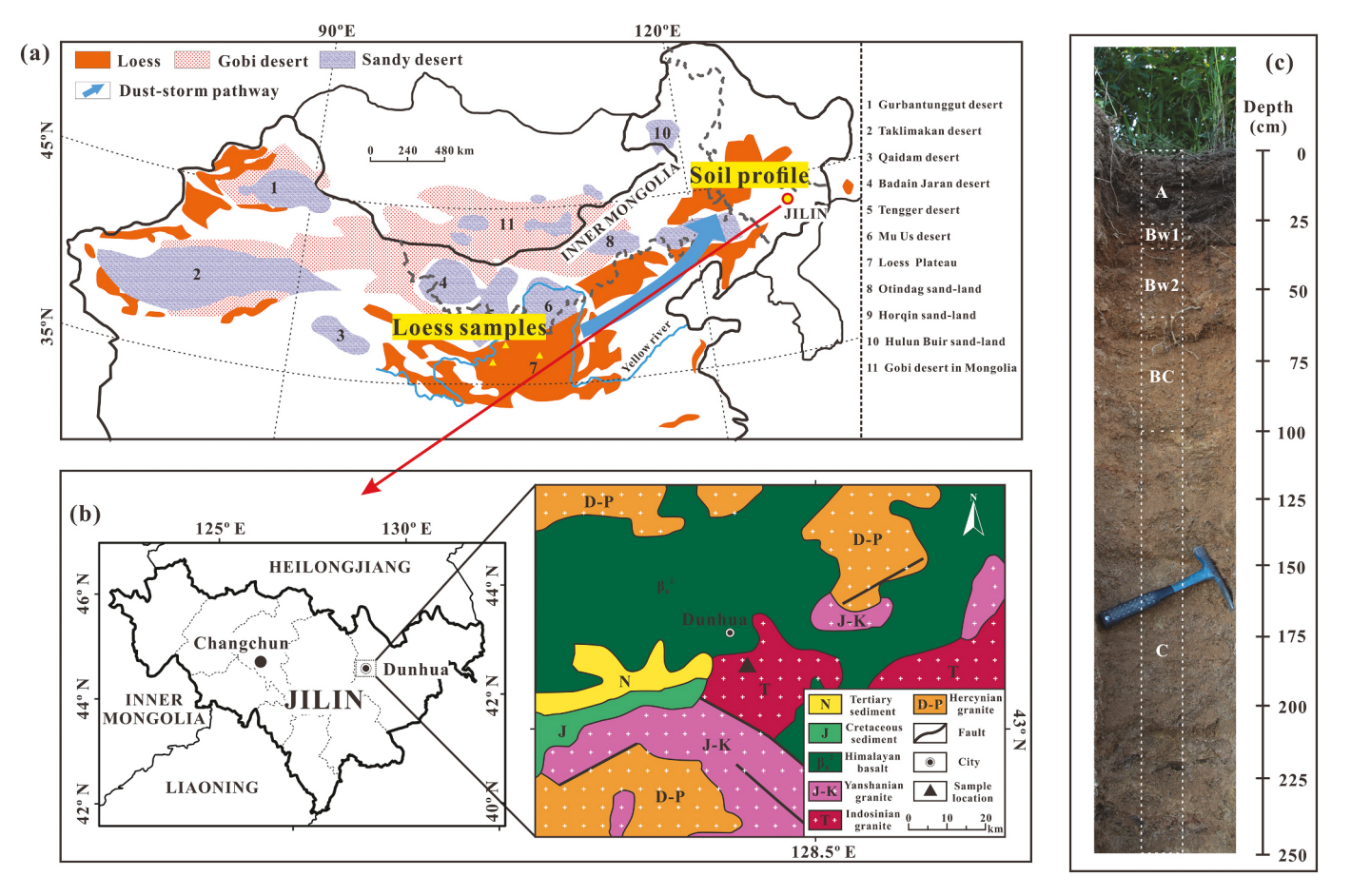


Fig. 1. (a) A sketch map showing the distribution of loess, Gobi deserts and sandy deserts in northern China and southern Mongolia (modified after Sun et al., 1998). The dust-storm transporting pathway is drawn based on meteorological record and back trajectories of moving path of dust particles at 250–1500-m heights (after Ma et al., 2013). Three loess samples were collected at Loess Plateau. (b) Site location and schematic geological map, and (c) a photo of the profile.

limited amount of synchrotron X-ray beamtime, only one soil profile was selected for P K-edge XANES analysis, and we only report other data associated with the profile as well. In addition, a visual inspection of the profile suggests that the interruption or abrupt changes in color, texture, and structure did not occur in the transition from bottom to topsoil of the profile (Fig. 1c); thus, we inferred that this profile developed continuously since it was exposed to weathering. Despite dust inputs, it did not change the general patterns of metal distribution in soil profiles resulted from in-situ weathering of granite protolith (Liu et al., 2016), i.e., increasing K and Na concentrations and decreasing Fe and Al concentration with increasing depth (Fig. S1).

The soils were sampled with fine depth intervals (5–10 cm) down to 250 cm. The profile was divided into five horizons: A (0–20 cm), Bw1 (20–30 cm), Bw2 (30–60 cm), BC (60–100 cm), and C (100–250 cm) (Table S1) according to the United States Soil Taxonomy (Soil Survey Staff, 2014). The soil of the profile was classified as Ustic Dystrocryepts (Soil Survey Staff, 2014). Two bedrock samples were collected from an outcrop located on the downslope of the hillslope (tens of meters away from the profile). The mineralogy proved that the sampled bedrock specimens can represent the parent rock of the studied profile (Table S2).

The denudation rate of the soil profile was reported to be 33 m/Myr based on a cosmogenic nuclide (26 Al, 10 Be) analysis of the 250–500 µm coarse size fraction that was mainly produced by in-situ weathering of granite (Cui et al., 2021). Dust inputs also carry coarse particles that, however, contribute <0.6% of total dust mass and are deemed not to affect the cosmogenic analysis for obtaining the denudation rate (Xie et al., 2015). The soil residence time (SRT) was the duration of time during which soil particles, generated from in-situ weathering, remain in a soil profile and can be calculated as the profile thickness divided by the denudation rate (Dere, 2014). Using the reported denudation rate (Cui et al., 2021), the SRT of the profile was calculated to be 76 kyr. Since dust inputs increase the soil thickness of the profile (Eger et al., 2012), the SRT is likely overestimated.

2.2. Bulk soil preparation and particle size separations

The soil samples were air-dried and passed through 2-mm mesh sieves. The $<\!2$ mm samples were used for measurements of soil pH and particle size composition, as well as particle-size separation. Subsamples of the sieved soils and the granite rock samples were ball-milled to $<\!200$ mesh (75 μm) for measuring concentrations of major elements, pedogenic Fe and Al minerals and soil organic carbon (SOC), and Sr isotopic composition. The ground soils were also used for modified Hedley sequential extractions and P K-edge XANES spectroscopic analysis.

To determine the influence of dust inputs on weathering of apatite in parent materials, we selected 4 depths from different horizons to perform particle-size separation: 0-5, 20-25, 50-60, and 180-190 cm. The fine earth (<2 mm) was separated into four particle-size fractions: clay ($<2 \mu m$), silt ($2-50 \mu m$), fine sand ($50-250 \mu m$), and coarse sand (250–2000 μm). The separation was performed following the previous method (Stemmer et al., 1998). Briefly, bulk air-dried soil samples were suspended in Milli-Q water (water/soil = 5:1, v/w) and dispersed by low-energy sonication. The fine sand (50-250 μm) and coarse sand $(250-2000 \, \mu m)$ particles were separated by manual wet sieving. The siltsize particles (2-50 µm) were obtained by centrifuging the remaining suspension at 150g for 2 min at 15 $^{\circ}$ C, which was repeated three times. The clay-size particles (0-2 µm) were separated by centrifuging the supernatant at 3900g and 15 °C for 30 min. Then the obtained size fractions of the soils were freeze-dried. All the particle-size fractions were ground to pass through a 200-mesh sieve prior to concentration measurements of total P and other major elements, as well as P K-edge XANES data collection.

2.3. Strontium isotopic composition

Strontium isotopic composition was used to quantify the dust mass contribution of soil in the profile because it is not much altered by weathering processes and can reflect the mixing of Sr derived from various isotopically different sources (e.g., Aciego et al., 2017; Borg and Banner, 1996; Capo et al., 1998; Chadwick et al., 1999; Li et al., 2016; Pett-Ridge et al., 2009). The Sr isotopic compositions of granite and continental dust contrast strongly (Aciego et al., 2017; Capo et al., 1998), providing a useful means of distinguishing between local and aeolian soil components. Soil and rock samples were digested using HNO₃ and HF, and the digested suspension was then taken to dryness. All samples were then dissolved in 1.5 M HCl and centrifuged to remove any trace insoluble residues, and the concentration of Sr was measured on a small aliquot of these solutions using inductively coupled plasmaoptical emission spectroscopy (ICP-OES, Perkin Elmer Optima 8300) with an accuracy of \leq 1%. Another aliquot of each solution was eluted through quartz cation exchange columns using Biorad AG50-WX8 200-400 mesh resin to separate a pure Sr fraction. Sr isotopic compositions were analyzed with a multiple-collector inductively coupled plasma-mass spectrometer (MC-ICP-MS; Nu Instruments, Wrexham, UK). Analyses of National Bureau of Standards (NBS) standard SRM 987 yielded a mean 87 Sr/ 86 Sr ratio of 0.710288 \pm 0.000020 (σ , n=20) (certified value: 0.710340 ± 0.000260) during the period of analyses. The column processed seawater yielded $^{87}\text{Sr}/^{86}\text{Sr} = 0.709198 \pm$ 0.000014 (σ , n = 8), identical to that reported by Mokadem et al. (2015). U.S. Geological Survey BHVO basalt, which was digested and analyzed in the same manner as the profile samples, yielded $^{87}Sr/^{86}Sr =$ 0.703540 ± 0.000017 (σ , n = 6), identical to that reported by Weis et al. (2006). The uncertainties of ⁸⁷Sr/⁸⁶Sr based on duplicate profile samples were estimated to be less than ± 0.000032 .

The mass fraction of dust-derived Sr (f_{dust}^{Sr}) in the profile was calculated using the following equation based on the Sr isotope mass balance (Kurtz et al., 2001).

$$f_{dust}^{Sr} = \frac{d_{soil} - d_{granite}}{d_{dust} - d_{granite}} \tag{1}$$

where d_{soil} , $d_{granite}$ and d_{dust} refer to the ⁸⁷Sr/⁸⁶Sr ratio of the soil, granite and continental dust, respectively.

The "bulk soil" Sr concentration for the profile was corrected by the loss on ignition (LOI wt%) that was determined by ashing soil samples for 5 h at 550 °C (Christensen and Malmros, 1982).

$$[Sr]_{bulk} = [Sr] \left(\frac{100 - LOI(wt\%)}{100} \right)$$
 (2)

The mass of dust-derived Sr (g/m²) was determined from the product of the mass fraction of dust-derived Sr (Eq. 1), bulk soil [Sr] (Eq. 2), soil dry bulk density ρ and profile thickness h.

$$Sr_{dust}^{mass} = f_{dust}^{Sr} \times [Sr]_{bulk} \times \rho \times h$$
 (3)

The mass of dust deposited in the profile was calculated by dividing the mass of dust-derived Sr by the Sr concentration in Asian dust (26 ppm, based on the Geochemical Earth Reference Model average for upper continental crust; see http://www-ep.es.llnl.gov/germ). The long-term average dust deposition rate, 2.25 $g/m^2/yr$, was then estimated by dividing the mass of dust deposited by SRT.

2.4. Soil physical and chemical characterization

The bulk density of each soil sample was determined using the core method (Blake and Hartge, 1986). A portion of each field-moist soil sample was weighed, oven-dried at $105\,^{\circ}\text{C}$ to equilibrium (in practice, over a 24 h period), and then re-weighed. The bulk density was calculated as the ratio of the mass of oven-dried soil to the volume of the sampler ($100\,\text{cm}^3$). Bulk soil pH was measured in $1:2.5\,\text{soil/CO}_2$ -free

deionized water suspensions using a glass electrode. The SOC concentrations were determined with an elemental analyzer (vario MACRO cube, ELEMENTAR) after decarbonation. In addition to the above particle size separation, the particle size composition of the bulk soils was determined using a Mastersizer 2000 (Malvern, UK) laser diffractometer, following a pretreatment with hydrogen peroxide to remove the organic component and chemical dispersion with sodium hexametaphosphate. The mineralogy of bulk soils was characterized using X-ray diffraction (XRD). The XRD data were collected using an amorphous silicon image plate at beamline 11-ID-B ($\lambda = 0.2115$ Å) at the Advanced Photon Source (APS), Argonne National Laboratory. Samples were mounted in 1-mm thick Kapton capillaries. Two dimensional images were integrated into intensity vs 20 plots using the program Fit2D (Hammersley et al., 1996). Detailed parameters used in the calibration and conversion were described in our previous study (Gu et al., 2019). The PROFEX software was used to identify and quantify the mineral phases in the samples (Doebelin and Kleeberg, 2015).

Major elements (Si, Al, Fe, Na, K, Mg, Ca, P and Ti) of the bulk soils and particle-size fractions were determined by ICP-OES after lithium tetraborate fusion at $1000~^{\circ}\text{C}$ for 60 min followed by 5% *aqua regia* digestion of the fusion beads (Robertson et al., 1999).

The mass transfer coefficient τ_{Fe} was used to evaluate the enrichment or depletion of Fe in the bulk soils relative to parent material (Nesbitt, 1979).

$$\tau_{Fe} = \left(\frac{[Fe]_w \times [Ti]_p}{[Fe]_p \times [Ti]_w} - 1\right) \times 100 \tag{4}$$

where [Fe] and [Ti] are the concentrations of Fe and the relatively immobile element Ti respectively, and the subscript w and p refer to the weathered soils and bedrock, respectively. The $\tau_{\rm Fe}$ indicates Fe depletion ($\tau_{\rm Fe} < 0$) or enrichment ($\tau_{\rm Fe} > 0$) relative to the composition of the bedrock. Note that using this equation to calculate mass balance assumes granite rock as the only parent material source. The influence of dust on mass balance calculations can be ignored when dust inputs do not alter the ratio of [Fe]/[Ti] in the bedrock (Lawrence et al., 2013). In this study, the ratio of [Fe]/[Ti] in the granite (8.1) was similar to that in the modern dust that deposited at the studied site (7.4–9.2) (Xie and Chi, 2016). Thus, Eq. 4 allows for rough estimates of the gain and loss of Fe in the profile (Bullen and Chadwick, 2015; Buss et al., 2017; Lawrence et al., 2013; Li et al., 2020; Rea et al., 2020).

Pedogenic Fe and Al minerals were assessed by a two-step extraction method using acidic (pH 3.2) ammonium oxalate solution (Fe $_{\rm ox}$, Al $_{\rm ox}$) (Schwertmann, 1964), followed by citrate-dithionite solution (Fe $_{\rm di}$, Al $_{\rm di}$) (Holmgren, 1967). The extracts were analyzed for Fe, Al and P concentrations by ICP-OES. The total contents of pedogenic Fe and Al (Fe $_{\rm ox+di}$, Al $_{\rm ox+di}$) were calculated as the sum of the oxalate and dithionite extracted Fe and Al. Phosphorous (P $_{\rm ox+di}$) associated with pedogenic Fe and Al was also extracted by the above two processes.

The degree of P saturation (DPS $_{ox}$) of each soil, defined as the ratio of the amount of adsorbed P to the P sorption capacity of the soil, was used to evaluate the potential of soils to release P (Hooda et al., 2000). DPS $_{ox}$ was calculated on a molar basis using the following formula:

$$DPS_{ox} = \frac{P_{ox}}{Al_{ox} + Fe_{ox}} \times 100 \tag{5}$$

The modified weathering potential index (MWPI) was used to quantify the degree of weathering based on the molecular ratio of major oxides, as calculated below (Vogel, 1975):

$$MWPI = \frac{Na_2O + K_2O + CaO + MgO}{Na_2O + K_2O + CaO + MgO + SiO_2 + Al_2O_3 + Fe_2O_3} \times 100$$
 (6)

The smaller value of MWPI indicates a greater degree of weathering and leaching loss.

2.5. Phosphorus K-edge XANES spectroscopy

Phosphorus K-edge XANES spectra were collected from the bulk soil samples and particle-size fractions at the Soft X-ray Micro-Characterization Beamline (SXRMB) at the Canadian Light Source, Saskatoon, Canada. The characteristics of the equipment and the scanning parameters were the same as used in our previous study (Gu et al., 2019; Zhang et al., 2021). Each sample was scanned twice or more, and the spectra were averaged to improve signal-to-noise ratios. The spectra were background removed, normalized and then subject to a linear combination fitting (LCF) analysis to quantify the relative proportions of various P species using ATHENA (Ravel and Newville, 2005). The following phosphate references, which were either purchased or synthesized according to the previous studies (Gu et al., 2019; Zhang et al., 2018; Zhang et al., 2021), were used for LCF spectral fitting, including poorly crystalline apatite (Ca-P), hydroxyl apatite (Ca-P), ferrihydriteadsorbed PO₄ (Fe-P), amorphous FePO₄ (Fe-P), kaolinite-adsorbed PO₄ (Al-P), and phytic acid sodium salt (organic P, P₀) (Fig. S2). Four or fewer P reference compounds were chosen for each fitting to prevent overfitting for the LCF analysis. No energy shift was allowed during the fitting. The obtained soil P species were grouped into three pools that are Ca-P, (Fe + Al)-P, and Po. The Ca-P pool comprises all Ca-P references used in the XANES fitting, and (Fe + Al)-P all Fe-P and Al-P references. These two pools correspond to inorganic P in soils.

2.6. Modified Hedley chemical extractions

We used the modified Hedley methods to extract the operationally-defined pools of P from bulk soils (Hedley et al., 1982; Tiessen and Moir, 1993). A soil sample (0.5 g) was sequentially extracted in duplicate with anion-exchange resin, 0.5 M NaHCO $_3$ (pH 8.5), 0.1 M NaOH and 1 M HCl (hereinafter referred to as "dHCl"), and concentrated HCl (hereinafter referred to as "cHCl"). After each extraction, the suspension was centrifuged and the supernatant was passed through a 0.45- μ m filter. The residual P after the cHCl extraction was determined by the lithium tetraborate fusion method (Robertson et al., 1999).

Total P (P_t) in dHCl and cHCl extracts was determined by ICP-OES. Aliquots from the filtered NaHCO $_3$ and NaOH extracts were digested in an autoclave at 103.5 kPa and 121 °C with ammonium persulfate to convert all the dissolved P into orthophosphate, which was then measured as P_t . The inorganic P (P_i) in all extracts and the P_t in NaHCO $_3$ and NaOH extracts were determined by the molybdenum blue method (Murphy and Riley, 1962), and P_o was calculated as the difference (P_t - P_i). The obtained fractions were combined to approximate P pools as follows (Cross and Schlesinger, 1995): Ca-P = dHCl- P_i ; non-occluded P ($P_{n\text{-}occ}$) = resin- P_i + NaHCO $_3$ - P_i + NaOH- P_o ; occluded P (P_{occ}) = cHCl- P_o . In addition, resin- P_i and NaHCO $_3$ - P_o + NaOH- P_o + dHCl- P_o - cHCl- P_o . In addition, resin- P_i and NaHCO $_3$ - P_i are also widely used as indicators of soil P bioavailability. The labile P_i pool was calculated as the sum of resin- P_i + NaHCO $_3$ - P_i , which is probably equivalent to Olsen P, a classical agronomic test for soil P availability (Sims, 2000).

2.7. Dust acidification treatment

To evaluate the susceptibility of dust-borne P to acidic dissolution in the acidic soils after deposition, we investigated the dust-borne P transformation using leaching experiments with 10% acetic acid solution (pH 4). It is difficult to obtain a dust sample to represent historical dust because modern dust might differ from dust deposited during the long history of soil development (Marx et al., 2018). Thus, in this study, three loess samples were used as surrogates of the dust deposited at our study site and collected from the surface soils of Loess Plateau and located in Tongxin, Ningxia; Wangjiashan, Gansu; and Huanxian, Gansu (Fig. 1a). The loess samples were air-dried and pooled to make one composite sample. The silt-sized loess from the Loess Plateau was reported to be the most important source of aeolian inputs for the study

sites during the long time period of soil development (Hoffmann et al., 2008; Shen et al., 2007; Xie et al., 2018b),

The loess sample was resuspended in a 10% acetic acid solution and mixed at 30 rpm on a rotator for 48 h. Every 12 h, the suspension was centrifuged, and the obtained supernatant was replaced by a fresh acetic acid solution, which was mixed by vortex prior to continuing mixing on the rotator. The solid residues collected at 12 h and 48 h by centrifugation, respectively, were subject to measurements of elemental composition and P K-edge XANES spectra.

2.8. Statistical analyses

To determine how P speciation determines P availability, potential correlations were explored between P availability indicators (i.e., resin-P_i, NaHCO $_3$ -P_i, and labile P $_1$) and XANES-derived P speciation and Hedley-derived P $_0$. A correlation analysis was also carried out between the indicators and DPS $_{ox}$. The correlations were assessed by regression analyses using Origin 2018.

3. Results

3.1. Dust mass contributions to soils

The dust mass contributions to soils were quantified using the Sr isotope analysis. The granitic bedrock had an average ⁸⁷Sr/⁸⁶Sr ratio of 0.70625 (Fig. 2a). Based on the reported Sr isotopic data of Asian dust (Chen and Li, 2013; Kanayama et al., 2002; Rao et al., 2006), we used a mean ⁸⁷Sr/⁸⁶Sr ratio of 0.7199 as the representative value of the continental dust (see SM-1). The entire profile had higher ⁸⁷Sr/⁸⁶Sr values than the bedrock, ranging from 0.71100 to 0.71355 (Fig. 2a). Based on Eq. (1), the soil mass fraction of dust-derived Sr in the profile was determined and ranged from 34.8% to 53.5% at different depths (Fig. 2b). The highest contribution of dust to soils in the Bw2 horizon may be attributed to the downward translocation of fine dust particles, as well as temporal variations in dust flux and composition during the soil profile development. Overall, the Sr isotopic composition suggests that aeolian dust inputs penetrate the deep soils and contribute

substantially to the soil mass at depths in the entire profile.

3.2. Soil properties

The MWPI, soil pH, SOC, τ_{Fe} value, pedogenic Fe and Al concentrations, and particle-size distributions are provided in Figs. 3 and 4. The MWPI value of the unweathered bedrock was 11.0 (Fig. 3a). The MWPI values of the soils at depths were substantially lower than that of the bedrock and varied slightly between 6.4 and 8.0 with depth (Fig. 3a). The MWPI value of highly weathered granite was reported to be about 6 (Lee et al., 2020). Thus, the soils in the entire profile were well weathered.

The soils were weakly to moderately acidic (Fig. 3b). The soil pH slightly increased from 5.3 at the surface to 5.5 at 10-cm depth, then decreased to 5.0 at 25-cm depth, and again gradually increased to 6.2 at the bottom. The SOC concentrations were the highest at the surface (32.4 mg/g) and declined rapidly to 5 mg/g around 30 cm, below which the concentration decreased slowly to the bottom (Fig. 3c).

The τ_{Fe} values were the lowest (~ 10%) in the A horizon and remained nearly constant (~ 43%) below 25-cm depth (Fig. 3d). Fe_{ox} and Fe_{di} accounted for 2.8–9.0% and 29.4–50.8% of total Fe, respectively (Fig. 3e, f). The proportion of Fe_{ox} to the total Fe was higher in the A and Bw1 horizons than in the underlying horizons. The proportion of Fe_{di} to the total Fe increased with increasing depth. Additionally, oxalate and dithionite extracted 33.7–60.8% of total P (Fig. 3g). The entire profile has low DPS_{ox} values, ranging from 1.9 to 5.8% (Fig. 3h).

The soil texture of the profile was dominated by fine sand (29.4–62.1%) and silt (28.9–61.8%) with minor clay (0.8–8.7%) and coarse sand (0–14.3%) (Fig. 4a-d). Both clay and silt fractions had higher proportions in the A and Bw1 horizons than in the underlying horizons, whereas both fine and coarse sand fractions showed reverse trends. Fig. 4e showed the particle-size frequency curves of the profile samples, which are consistent with the soil texture results.

3.3. Phosphorus concentration, speciation, and pools in bulk soils

Total P concentrations were the highest (379-411 µg/g) in the A

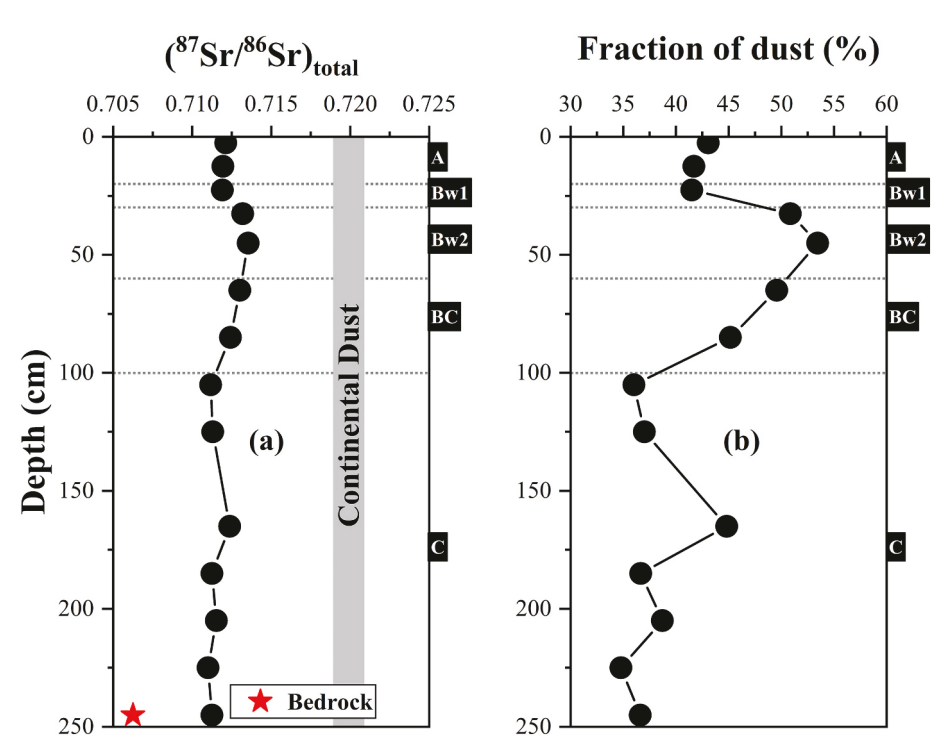


Fig. 2. The ⁸⁷Sr/⁸⁶Sr ratios (a) and the dust mass contributions (b) as a function of soil depth in the soil profile.

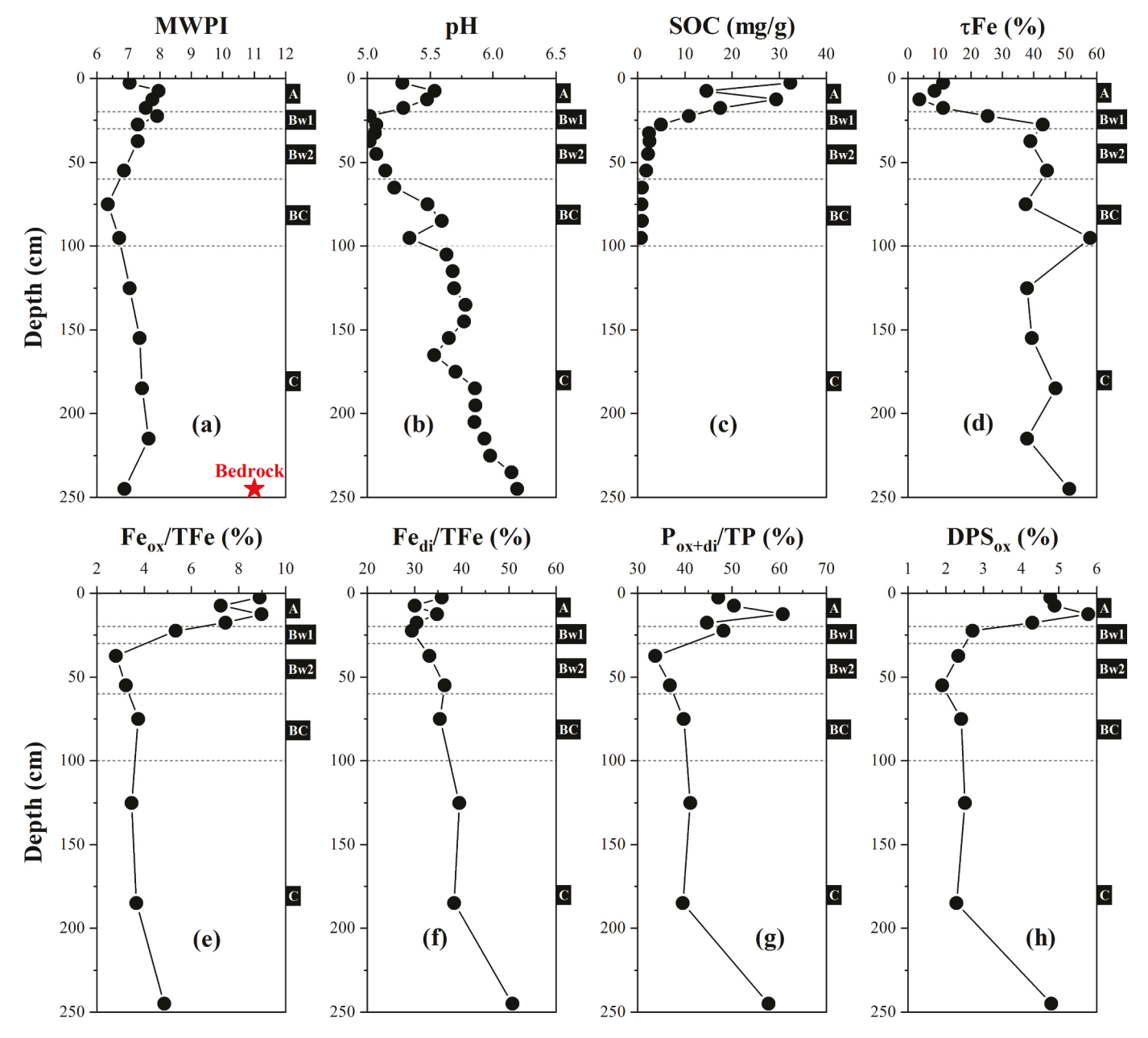


Fig. 3. Depth-dependent modified weathering potential index (MWPI) (a), pH (b), soil organic carbon (SOC) concentration (c), τ_{Fe} (d), percentages of oxalate (e) and dithionite extractable Fe of total Fe (f), percentages of P_{ox+di} of total P (g), and degree of P saturation (DPS_{ox}) (h).

horizon, substantially lower (180–239 $\mu g/g$) in the B horizons whereas it remained nearly constant (172–225 $\mu g/g$) in the C horizon (Fig. 5a, Table S4). The total P concentrations in B and C horizons were lower than that of bedrock (295 $\mu g/g$).

Phosphorus K-edge XANES spectroscopy was used to characterize the speciation of inorganic P in the soil samples based on the type of metal bound to PO4. According to the LCF analysis, the proportion of (Fe + Al)-P ranged from 57 to 83% of total P and that of Ca-P from 4 to 18% in the profile (Fig. 5b, Table S5). The Ca-P proportions decreased from the surface to the B horizons and then increased towards the bottom of the profile. The (Fe + Al)-P proportions increased from the surface to the B horizons and remained nearly constant below that depth.

To assess P availability, soil P was fractionated into different pools using the modified Hedley sequential extractions (Fig. 5c, d, Table S4). Labile P_i (sum of resin- and NaHCO₃- P_i), which is considered readily available for plants, constituted a small proportion of total P across the entire profile (0.5–7.4%). The proportion of labile P_i over total P

decreased from surface (5.3%) to B horizons (< 1%) and then increased towards the bottom (7.4%) of the profile. A similar pattern was observed for NaOH-P; (4.0-15.0%) that is defined as inorganic P adsorbed to secondary Fe/Al minerals. The sum of labile P_i and NaOH-P_i, representing the P_{n-occ} pool in the Walker and Syers model (Cross and Schlesinger, 1995), constituted 5.3–22.4% of total P. The Pocc pool (sum of cHCl-P_i and residual-P), assumed to be P strongly bound to Fe and Al and/or physically protected, was the dominant form (43.6-84.5%) across the profile. dHCl-Pi, which is considered to be mainly Ca-P and may include some (Fe + Al)-P occluded by poorly crystalline Fe and Al oxides (Gu et al., 2020), constituted a small proportion (4.9-14.6%) of total P across the profile. In addition, the Po pool (sum of NaHCO3-Po, NaOH-P_o, dHCl-P_o, and cHCl-P_o) decreased from 33.7% at the surface to 11.3% at the bottom of the profile. The difference of Po fractions determined between the XANES-LCF and chemical extraction analyses was less than 10% (Fig. S5), which can be attributed to the uncertainty of the XANES fitting (Ajiboye et al., 2007; Zhang et al., 2021).

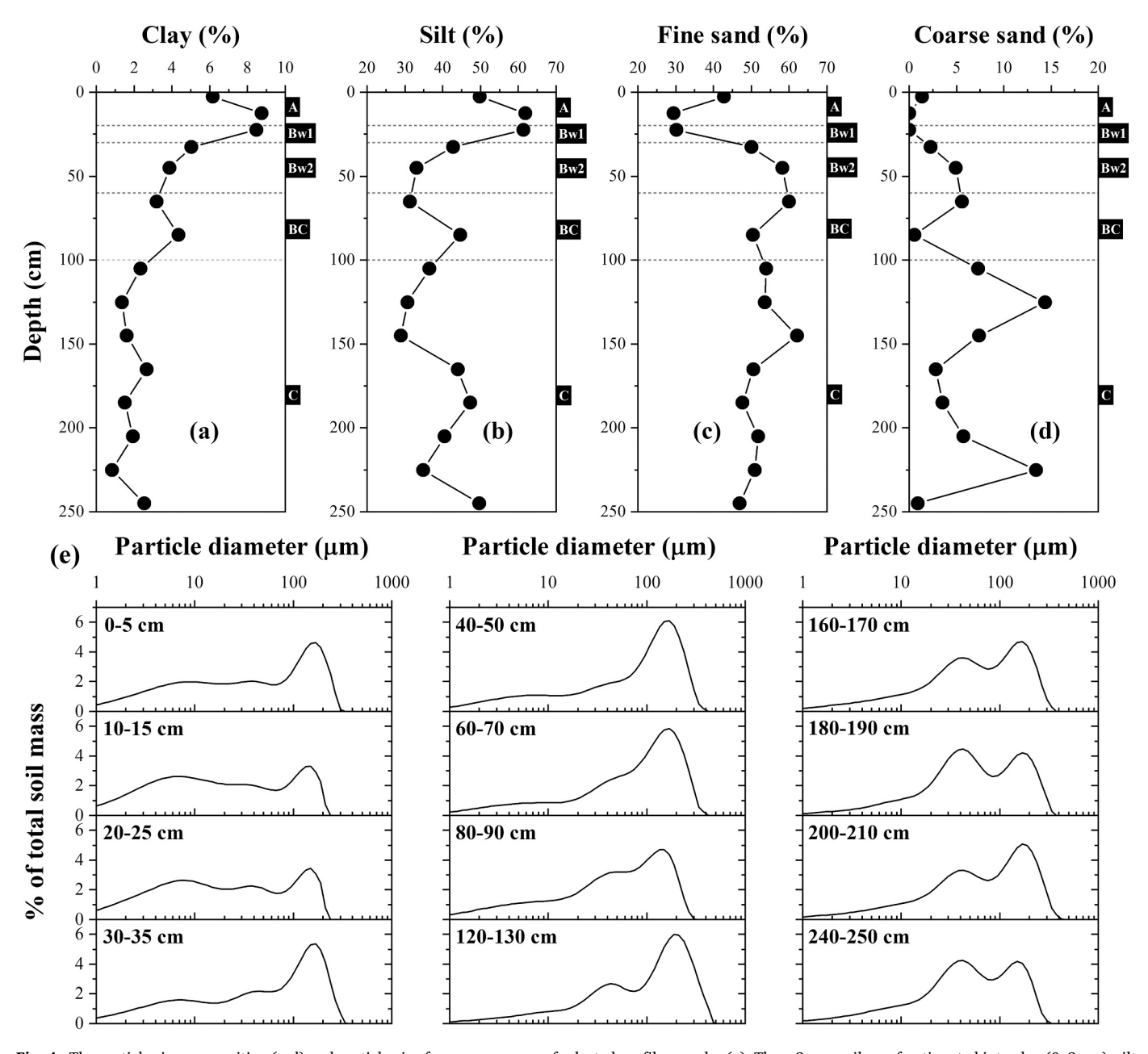


Fig. 4. The particle size composition (a-d) and particle-size frequency curves of selected profile samples (e). The <2 mm soil was fractionated into clay (0-2 μ m), silt (2-50 μ m), fine sand (50-250 μ m) and coarse sand (250-2000 μ m) fractions.

3.4. Phosphorus speciation in particle-size fractions

The P speciation of different particle-size fractions was further characterized to examine the influence of dust inputs on P geochemistry in soils (Fig. 6, Table S6). The P speciation in the coarse sand fraction of the surface soil was composed of 25% Ca-P, 41% (Fe + Al)-P and 34% P_o , whereas the P speciation in the fractions of B and C horizons was dominated by (Fe + Al)-P (94–100%) with negligible Ca-P (0–2%) (Fig. 6d). The P speciation of the fine sand fraction varied slightly with depth, consisting of 3–14% Ca-P, 68–83% (Fe + Al)-P, and 6–18% P_o (Fig. 6c). The low Ca-P in the two sand fractions was consistent with the barely observed Ca-P spectral features (Fig. S4). Note that the obtained Ca-P proportions in the fine and coarse sand fractions of the C horizon sample (180–190 cm) may have large uncertainties due to the low spectral quality caused by their low P concentrations (R-factor > 0.01, Table S6). As to the finer size fractions, the clay and silt fractions showed similar P speciation, consisting of 0–10% Ca-P, 76–93% (Fe + Al)-P and

7-19% Po (Fig. 6a, b).

3.5. Solubility of dust-borne P during acidic leaching

The acidic leaching experiment at pH 4 was performed on the dust sample to determine how the speciation and availability of dust-borne P would change after deposition into acidic soils. The dust residue after 12 h and 48 h leaching with 10% acetic acid solution showed slightly higher concentrations of Si, Al, Fe, K and Mg than the untreated loess (Fig. 7a, Table S7). However, Ca and P showed significant decreases in the dust residues compared with the untreated dust. Thus, Ca and P were preferentially leached into solution compared to other elements. The acidification substantially changed the P speciation of the dust. The XANES spectra of the untreated dust sample and residue after 12-h leaching exhibited the strong Ca-P features, while the spectrum of the residue of 48-h treatment resembled the Fe-P spectra (Fig. 7b). Consistently, the LCF results showed that the untreated dust sample and residue after 12-h

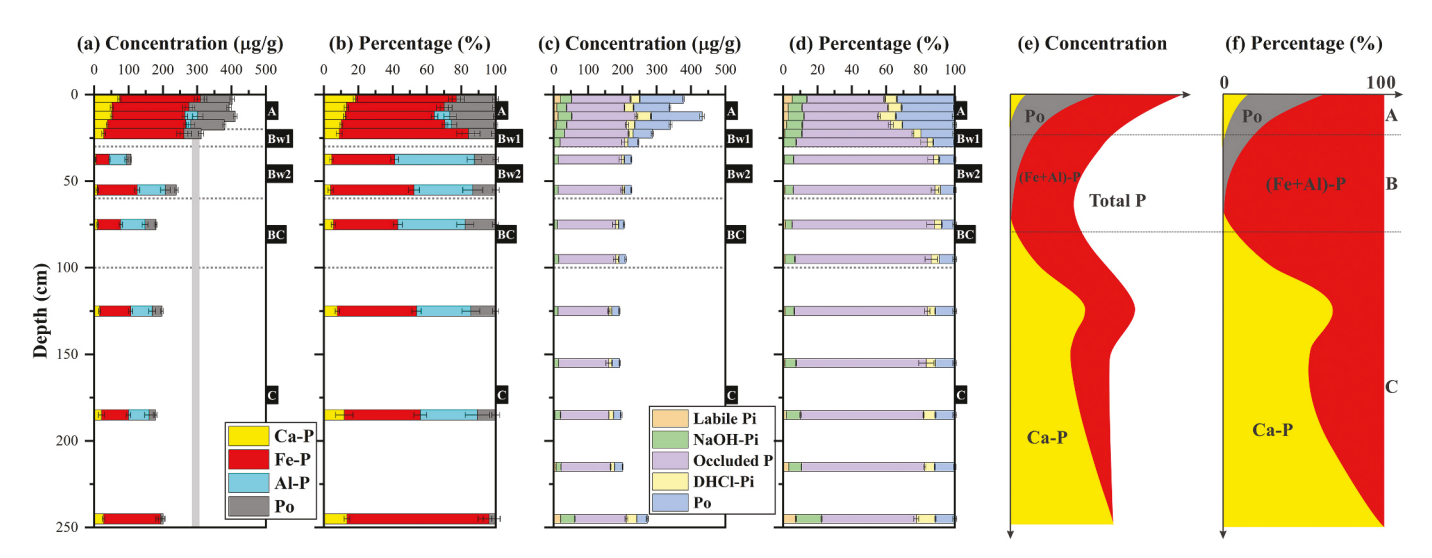


Fig. 5. The concentrations and proportions of various XANES-derived P species (a and b) and the operationally-defined P pools based on the modified Hedley fractionations (c and d) for the soil profile. The grey bar in (a) indicates the P concentration of the bedrock. The vertical patterns of P concentration and speciation in soil profiles were proposed by Zhang et al. (2021) and they were less affected by dust inputs than the profile in the present study (e, f).

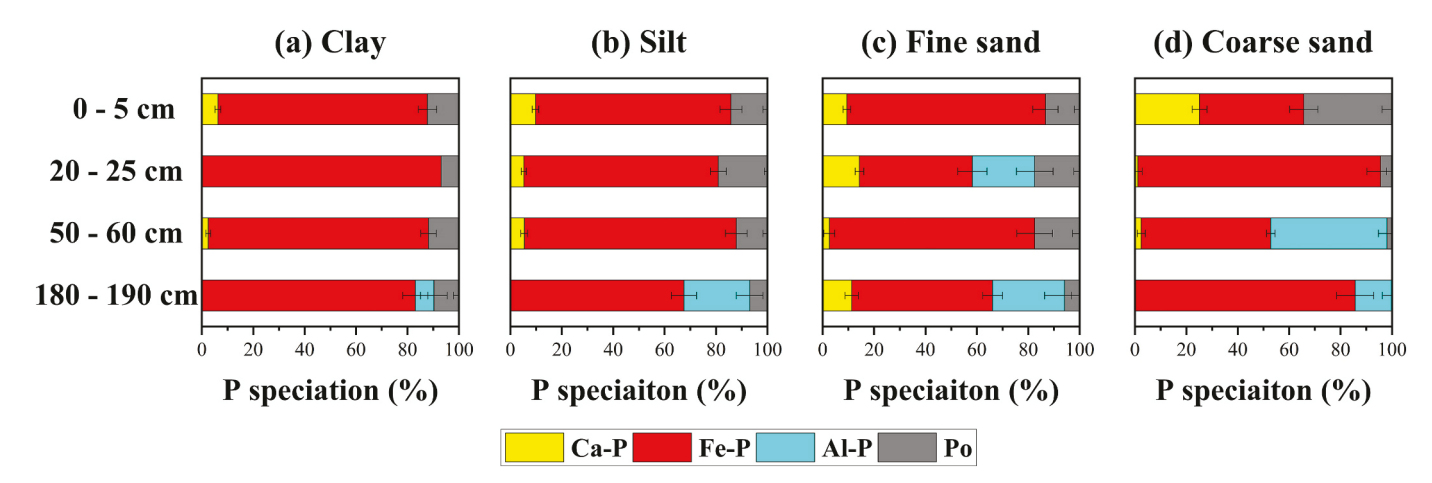


Fig. 6. The XANES-derived P speciation of particle-size fractions.

leaching had similar Ca-P percentages (51% and 48%, respectively), which dropped to 0% at 48-h (Fig. 7c, Table S8). This indicates that dust-borne Ca-P compounds were highly susceptible to acidic dissolution.

3.6. Correlations of P availability with P speciation and DPS_{0x}

To understand how dust affects P availability, we further explored correlations of P availability with P speciation, P_0 and DPS $_{ox}$ (Fig. 8). The proportions of resin- P_i , NaHCO $_3$ - P_i , and labile P_i correlated significantly and positively with the XANES-derived Ca-P proportions ($R^2 = 0.64$ –0.98, p < 0.005, Fig. 8a-c), Hedley-derived P_0 ($R^2 = 0.31$ –0.57, p < 0.038, Fig. 8g-i), and DPS $_{ox}$ ($R^2 = 0.41$ –0.68, p < 0.045, Fig. 8j-l) but negatively with (Fe + Al)-P ($R^2 = 0.48$ –0.82, p < 0.022, Fig. 8d - f). In addition, P_{occ} correlated positively with (Fe + Al)-P in proportion ($R^2 = 0.9$, p = 0.00003) (Fig. 8m).

4. Discussion

4.1. Phosphorus speciation and concentration in topsoils

The observed P speciation and concentration distribution as a function of depth in the topsoils (Fig. 5) are typical to forest ecosystems (Zhang et al., 2021). With increasing depth in the topsoils, total P

concentration decreases, and both Ca-P and P_o decrease and (Fe + Al)-P increase in proportion (Fig. 5a, b). A conceptual model to describe the vertical patterns of P concentration and speciation was proposed previously by Zhang et al. (2021), as shown in Fig. 5e and f. Those profiles were less affected by dust inputs than the profile in the present study. The patterns can be ascribed to inputs of alkaline, calcareous and Ca-P rich dust materials, weathering, plant biolifting of P from B to overlying A horizon, and downward P leaching and particle translocation (Zhang et al., 2021).

The dust inputs are likely the primary source of the observed Ca-P in the acidic topsoils. Ca-P was essentially absent in soils with soil pH < 5.5 because Ca-P compounds are highly susceptible to acidic dissolution in this pH range (Andersson et al., 2016; Zhang et al., 2021). Indeed, the acidic leaching experiment demonstrates that dust-borne Ca-P can be completely dissolved at pH 4 within 48 h (Fig. 7c). Phosphate leaching with even higher pH (pH 5) was observed previously for mineral dust deposited to Cape Verde islands and the Rocky Mountains in Colorado (Dam et al., 2021; Zhang et al., 2018). The presence of considerable Ca-P (4–24% of the total inorganic P pool, Fig. S6) in the topsoils of pH 5–5.5 can be ascribed to the continuous dust inputs, bringing new Ca-P to the system (Vogel et al., 2021). The Ca-P pool in the topsoils likely reaches a steady state where the rate of Ca-P accrual due to dust inputs is equal to the rate of Ca-P removal by weathering and other processes. The

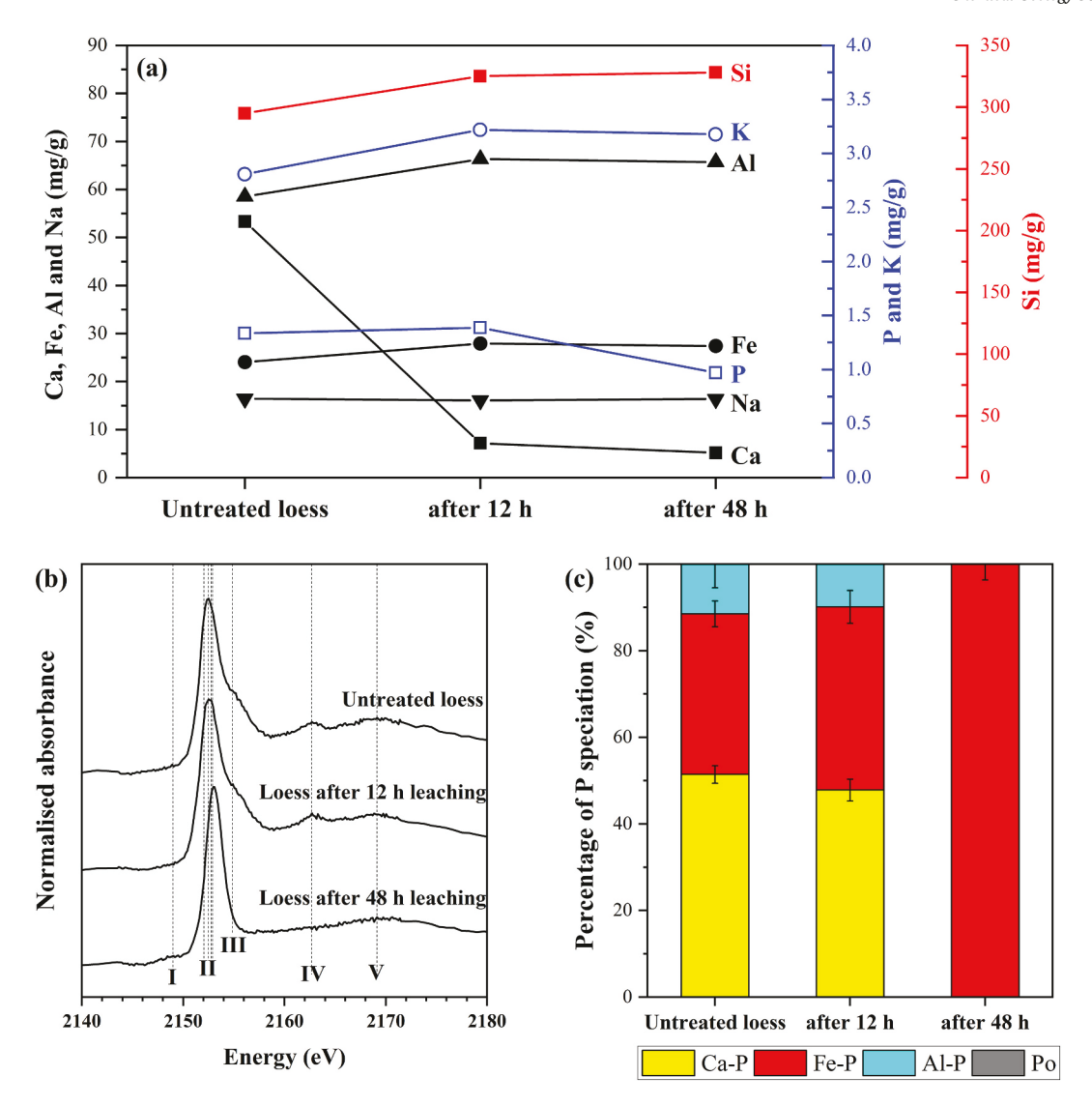


Fig. 7. The elemental concentrations of the loess residue before and after 12 h and 48 h leaching using 10% acetic acid (a), P K-edge XANES spectra of the loess residues (b), and the P speciation determined by a linear combination fitting analysis of the XANES spectra (c). The dashed lines in (b) indicate spectral features for different P species: (I) Fe-P, (II) white-lines, (III)-(V) Ca-P.

observed P speciation pattern in the topsoils (Fig. 5) is likely at a steady state as well.

The relatively low Ca-P proportions (25%) of the coarse sand fractions of the topsoils suggest ongoing weathering of dust-borne Ca-P minerals. The coarse sand grains that bear the Ca-P minerals in the topsoils must originate from aeolian dust inputs. In-situ weathering of granite at the site is unable to produce sand grains containing that high level of Ca-P in the acidic topsoils because apatite is relatively soluble and depleted in the early stage of weathering (Liu et al., 2016) and because the soils are old and the forest ecosystem has a strong weathering capability. A coarser size fraction usually has a higher Ca-P proportion than the bulk because of its lower weathering degree (Dam et al., 2021; Guo et al., 2011; Liu et al., 2014). However, the Ca-P proportions of the coarse sand grains are much lower than those of previously studied bulk dusts (47-92%) (Chen et al., 2006; Dam et al., 2021; Zhang et al., 2018) and the loess sample (42-74%) (Guo et al., 2011), suggesting that the sand grains have lost Ca-P via weathering substantially. Compared to the coarse sand fraction, other fractions of smaller particle sizes in topsoils generally have lower Ca-P proportions (<10%) (Fig. 6) probably because of their originally low Ca-P (Dam et al., 2021; Guo et al., 2011; Liu et al., 2014) and their larger specific surface areas that favor weathering after incorporation into soils.

Note that large sand-sized soil particles (up to 450 μ m) can be transported across a long distance by complex meteorological processes, such as the transport of Saharan coarse sand dust particles to the Atlantic Ocean 2400–3500 km away from West Africa (van der Does et al., 2018). Our study site is only 200–2000 km away from the dust source area (Fig. 1a) and thus has a high chance of receiving inputs of coarse dust particles. Indeed, Xie et al. (2015) showed that 0.1–0.6% coarse sand particles (250–500 μ m) existed in the aeolian dust deposition at a site geographically near ours.

4.2. Phosphorus speciation and concentration in C horizon soils

Neither P concentration nor speciation in the C horizon soils follow the typical patterns observed previously as shown in Fig. 5e and f. The most remarkable characteristics are the very low Ca-P proportions (< 13%, Fig. 5b), in contrast to the high Ca-P fractions previously observed in poorly weathered C horizon soils receiving little dust inputs in wetter and warmer environment (Zhang et al., 2021). The high weathering of the C horizon soils almost depleted all apatite in the coarse sand fractions that likely result from in-situ weathering of granite bedrock (Fig. 6d). The relatively high weathering degree could be due to increased soil moisture caused by dust inputs that enhance weathering

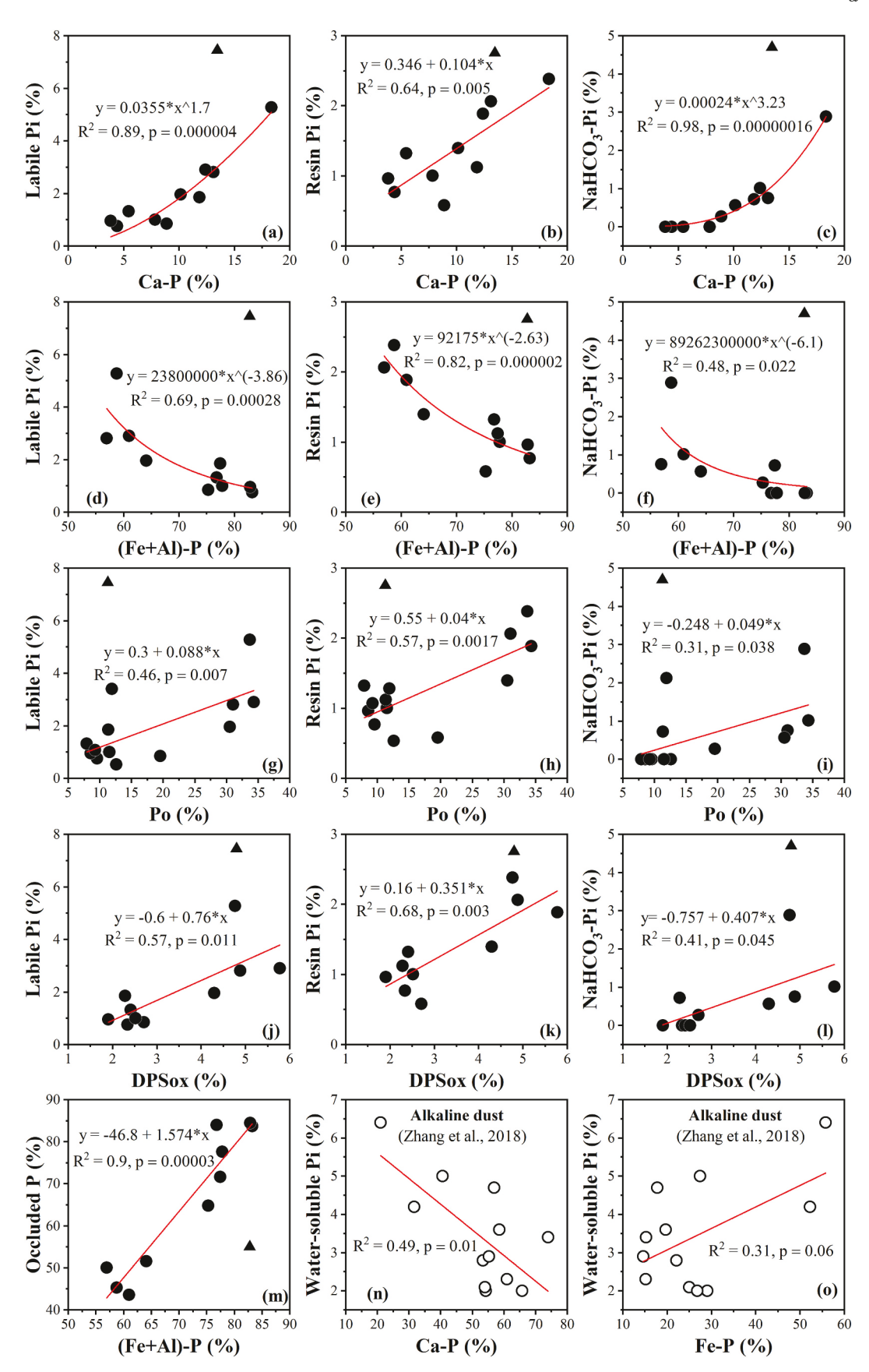


Fig. 8. Correlations of P availability indicators (i.e., labile P_i , resin- P_i , and NaHCO₃- P_i) with XANES-derived Ca-P (a-c), (Fe + Al)-P (d-f), Hedley-derived P_o (g-i) and DPS_{ox} (j-l), and correlation of occluded P with (Fe + Al)-P (m) for the profile samples. One outlier marked by triangle (240–250 cm) was excluded from the regression analyses in (a-m). The correlations of water-soluble P_i with XANES-derived Ca-P and Fe-P for short-distance transported alkaline mineral dust collected in the Rocky Mountains of Colorado, USA were reported by Zhang et al. (2018) (n, o).

in the relatively dry environment (Harden et al., 1991; Rasmussen et al., 2017). In addition, downward-moving dust particles may adsorb organic matter from the forest floor and deliver it to deep soils (Eger et al., 2013) to boost microbial activities there to enhance weathering (Buss et al., 2010). This postulation is supported by the presence of high P_0 in the C horizon soils (\sim 11%, Fig. 5d), which, however, was not detected in C horizon soils of forest soil profiles receiving little dust inputs (Zhang et al., 2021). Leaching may also transport organics to deep soils, as observed in the tropical climate (Zhang et al., 2021), which is likely limited here due to the low water availability.

4.3. Dust control of P bioavailability in soils

Phosphorus bioavailability in the soil profile is strongly influenced by aeolian dust inputs. With increasing soil depth, the labile P_i proportion (resin-P_i + NaHCO₃-P_i) decreases and reaches minimum at the B horizon before increasing towards the C horizon, similar to the Ca-P proportion (Fig. 5). The Ca-P proportions correlated with the proportions of labile P_i proportions, resin-P_i and NaHCO₃-P_i (Fig. 8a-c). Since Ca-P in the topsoils originate from aeolian dust inputs and that in the deep soils from bedrock, we can conclude that dissolution of dustborne Ca-P and bedrock Ca-P minerals are, respectively, responsible for the relatively high P availability at the surface and bottom of the profile. The stronger correlation of the P availability with Ca-P (Fig. 8ac) than Po (Fig. 8g-i), suggests that dissolution of Ca-P minerals is more important than mineralization of organic P in supplying available phosphate in these soils. Previous studies also suggest that dust inputs supply available P to tropical rainforests, but the contribution of dustborne P to the labile P_i pool was not directly observed, and the available forms of dust-borne P were not specified (Crews et al., 1995; Eger et al., 2013). They were not observed probably because tropical rainforests do not receive as much dust inputs as the sub-humid forest in the present study, and because organic P mineralization is the primary mechanism to supply available P in tropical soils (Johnson et al., 2003; Vincent et al., 2010).

Labile P_i and Ca-P do not always positively correlate to each other. Instead, Zhang et al. (2018) found that water-soluble P_i (similar to resin- P_i) negatively correlated with Ca-P but positively correlated with (Fe + Al)-P for short-distance transported alkaline mineral dust collected in the Rocky Mountains of Colorado, USA (Fig. 8n, o). The inconsistency is likely because Ca-P is unstable in the acidic soil as in the present study but stable in the alkaline aeolian dust, and vice versa for (Fe + Al)-P. A more quantitative relationship between the stability of Ca-P or (Fe + Al)-P and pH is reported in our previous study (Zhang et al., 2021). Therefore, dust-borne Ca-P can be effectively used by biota in sub-humid or wetter environment with acidic soils (pH < 5.5) but not in semiarid or arid environment characterized by circumneutral and alkaline soils (also including alkaline marine environment), which is opposite for dust-borne (Fe + Al)-P.

Another feature about the P availability in these soils is the dominance of occluded P, particularly in B horizons (Fig. 5d). The correlation between P_{occ} and (Fe + Al)-P (Fig. 8m) is consistent with the notion that Fe and Al oxides are primarily responsible for the occlusion. The occlusion largely limits the P availability although occluded P can be utilized by organisms with special P acquisition strategies (Cahill and McNickle, 2011; Lang et al., 2016). The dominance of occluded P is consistent with the high level of pedogenic Fe (34.7–55.6% of total Fe, Fig. 3e, f) throughout the profile that can be attributed to the inputs of Fe-rich aeolian dusts. Aeolian dust inputs in this geographic region (25-45 mg/g, e.g., Xie and Chi, 2016; Xie et al., 2018a) typically have several times higher Fe concentration than the granitic bedrock (12.2 mg/g) at the study site. The low DPS $_{ox}$ values further indicate that Fe/Al oxides in the soils are far from saturation with P adsorption and have a high potential to adsorb additional P from soil solution (Fig. 3h), which can further decrease P availability. In fact, a strong correlation exists between DPSox and P availability (Fig. 8j-l). Overall, pedogenic Fe and

Al oxides can adsorb released P from dissolution of dust-borne Ca-P and further regulate P availability.

5. Conclusions

Given that dust inputs are predicted to increase as climate warms and land-use intensifies and thus are increasingly important for supplying P to terrestrial ecosystems, it is important to understand the postdeposition fate of dust-borne P and how it becomes available in soils. Our study shows that in a sub-humid forest, aeolian dust inputs are the major supply of available P via acidic dissolution of dust-borne Ca-P minerals, and probably also enhance bedrock weathering in saprolite to enhance P release and availability. On the other hand, aeolian dust inputs lead to a high content of soil Fe oxides that can adsorb and occlude P to decrease its availability in a long term. Therefore, aeolian dust inputs affect P availability and dynamics in water-limited terrestrial ecosystems not only through acting as a P source but also through altering soil chemistry and bedrock weathering. Our findings also imply that the importance of dust-borne P to the available P pool in a dust-receiving ecosystem depends on both the chemical speciation of the dust-borne P and the pH of the ecosystem, as previously suggested for aquatic ecosystems (Dam et al., 2021; Zhang et al., 2018).

Declaration of Competing Interest

The authors declare that they have no known competing financial interests or personal relationships that could have appeared to influence the work reported in this paper.

Acknowledgement

This work was funded by U.S. National Science Foundation Faculty Early Career Development Program (EAR-1752903). Partial support was from the Roy J. Shlemon Center for Quaternary Studies at the University of Wyoming. Z. Zhang also thanks the support from the Chinese Scholarship Council. C. Liu and Z. Zhao thank the support from the National Natural Science Foundation of China (Grant Nos. 41930863, 41661144042, 41130536). We thank H. Ding, T. Liu, C. Tu, and B. Fan for collecting the soil samples used in this study. The authors are grateful to Dr. Karen L. Vaughan and Ph.D. student Than Dam in the Department of Ecosystem Science and Management at the University of Wyoming for their assistance in identifying soil horizons. The authors thank the beamline scientist Qunfeng Xiao at the Canadian Light Source for providing technical support during P K-edge XANES data collection. Canadian Light Source is supported by the Natural Sciences and Engineering Research Council of Canada, the National Research Council Canada, the Canadian Institutes of Health Research, the Province of Saskatchewan, Western Economic Diversification Canada, and the University of Saskatchewan. Use of the Advanced Photon Source, Argonne National Laboratory is supported by U.S. DOE-BES under Contract DEAC02-06CH11357.

Appendix A. Supplementary data

Supplementary data to this article can be found online at https://doi.org/10.1016/j.chemgeo.2021.120628.

References

Aciego, S.M., Riebe, C.S., Hart, S.C., Blakowski, M.A., Carey, C.J., Aarons, S.M., Dove, N. C., Botthoff, J.K., Sims, K.W.W., Aronson, E.L., 2017. Dust outpaces bedrock in nutrient supply to montane forest ecosystems. Nat. Commun. 8, 14800.
Ajiboye, B., Akinremi, O.O., Jürgensen, A., 2007. Experimental validation of quantitative

XANES analysis for phosphorus speciation. Soil Sci. Soc. Am. J. 71 (4), 1288–1291. Andersson, K.O., Tighe, M.K., Guppy, C.N., Milham, P.J., McLaren, T.I., Schefe, C.R., Lombi, E., 2016. XANES demonstrates the release of calcium phosphates from alkaline Vertisols to moderately acidified solution. Environ. Sci. Technol. 50 (8), 4229–4237.

- Blake, G.R., Hartge, K.H., 1986. Bulk density. In: Klute, A. (Ed.), Methods of Soil Analysis: Part 1. Physical and Mineralogical Methods. Soil Science Society of America, Madison, pp. 363–382.
- Borg, L.E., Banner, J.L., 1996. Neodymium and strontium isotopic constraints on soil sources in Barbados, West Indies. Geochim. Cosmochim. Acta 60 (21), 4193–4206.
- Bullen, T., Chadwick, O., 2015. Evidence for nutrient biolifting in Hawaiian climosequence soils as revealed by alkaline earth metal stable isotope systematics. Proced. Earth Planet. Sci. 13, 312–315.
- Buss, H.L., Mathur, R., White, A.F., Brantley, S.L., 2010. Phosphorus and iron cycling in deep saprolite, Luquillo Mountains, Puerto Rico. Chem. Geol. 269 (1–2), 52–61.
- Buss, H.L., Chapela Lara, M., Moore, O.W., Kurtz, A.C., Schulz, M.S., White, A.F., 2017. Lithological influences on contemporary and long-term regolith weathering at the Luquillo critical Zone Observatory. Geochim. Cosmochim. Acta 196, 224–251.
- Cahill, J.F., McNickle, G.G., 2011. The behavioral ecology of nutrient foraging by plants. Annu. Rev. Ecol. Evol. Syst. 42 (1), 289–311.
- Capo, R.C., Stewart, B.W., Chadwick, O.A., 1998. Strontium isotopes as tracers of ecosystem processes: theory and methods. Geoderma 82 (1–3), 197–225.
- Chadwick, O.A., Derry, L.A., Vitousek, P.M., Huebert, B.J., Hedin, L.O., 1999. Changing sources of nutrients during four million years of ecosystem development. Nature 397 (6719), 491–497.
- Chen, H.-Y., Fang, T.-H., Preston, M.R., Lin, S., 2006. Characterization of phosphorus in the aerosol of a coastal atmosphere: using a sequential extraction method. Atmos. Environ. 40 (2), 279–289.
- Chen, Z., Li, G., 2013. Evolving sources of eolian detritus on the Chinese Loess Plateau since early Miocene: Tectonic and climatic controls. Earth Planet. Sci. Lett. 371-372, 220–225
- Christensen, B.T., Malmros, P.Å., 1982. Loss-on-Ignition and carbon content in a beech forest soil profile. Holarct. Ecol. 5 (4), 376–380.
- Crews, T.E., Kitayama, K., Fownes, J.H., Riley, R.H., Herbert, D.A., Muellerdombois, D., Vitousek, P.M., 1995. Changes in soil phosphorus fractions and ecosystem dynamics across a long chronosequence in Hawaii. Ecology 76 (5), 1407–1424.
- Cross, A.F., Schlesinger, W.H., 1995. A literature review and evaluation of the Hedley fractionation: applications to the biogeochemical cycle of soil phosphorus in natural ecosystems. Geoderma 64 (3–4), 197–214.
- Cui, L., Yang, Y., Xu, S., Zhao, Z., Mao, H., Zhang, X., Tu, C., Zhang, Z., Liu, W., Liu, C., 2021. Denudation rates of granitic regolith along climatic gradient in Eastern China. Geomorphology 390, 107872.
- Dai, A., 2013. Increasing drought under global warming in observations and models. Nat. Clim. Chang. 3 (1), 52–58.
- Dam, T.T.N., Angert, A., Krom, M.D., Bigio, L., Hu, Y., Beyer, K.A., Mayol-Bracero, O.L., Santos-Figueroa, G., Pio, C., Zhu, M., 2021. X-ray spectroscopic quantification of phosphorus transformation in Saharan dust during trans-Atlantic dust transport. Environ. Sci. Technol. 55 (18), 12694–12703.
- Dere, A.L., 2014. Shale Weathering Across a Latitudinal Climosequence. The Pennsylvania State University, pp. 1–302.
- Pennsylvania State University, pp. 1–302.

 Doebelin, N., Kleeberg, R., 2015. Profex: a graphical user interface for the Rietveld refinement program BGMN. J. Appl. Crystallogr. 48 (5), 1573–1580.
- van der Does, M., Knippertz, P., Zschenderlein, P., Giles Harrison, R., Stuut, J.-B.W., 2018. The mysterious long-range transport of giant mineral dust particles. Sci. Adv. 4 (12), eaau2768.
- Eger, A., Almond, P.C., Condron, L.M., 2012. Upbuilding pedogenesis under active loess deposition in a super-humid, temperate climate—quantification of deposition rates, soil chemistry and pedogenic thresholds. Geoderma 189, 491–501.
- Eger, A., Almond, P.C., Condron, L.M., 2013. Phosphorus fertilization by active dust deposition in a super-humid, temperate environment—Soil phosphorus fractionation and accession processes. Global Biogeochem. Cycl. 27 (1), 108–118.
- Elser, J.J., Bracken, M.E., Cleland, E.E., Gruner, D.S., Harpole, W.S., Hillebrand, H., Ngai, J.T., Seabloom, E.W., Shurin, J.B., Smith, J.E., 2007. Global analysis of nitrogen and phosphorus limitation of primary producers in freshwater, marine and terrestrial ecosystems. Ecol. Lett. 10 (12), 1135–1142.
- Filippelli, G.M., 2008. The global phosphorus cycle: past, present, and future. Elements 4 (2), 89–95.
- Föllmi, K., 1996. The phosphorus cycle, phosphogenesis and marine phosphate-rich deposits. Earth Sci. Rev. 40 (1–2), 55–124.
- Gallardo, A., Fernández-Palacios, J.M., Bermúdez, A., de Nascimento, L., Durán, J., García-Velázquez, L., Méndez, J., Rodríguez, A., 2020. The pedogenic Walker and Syers model under high atmospheric P deposition rates. Biogeochemistry 1–17.
- Gu, C., Hart, S.C., Turner, B.L., Hu, Y., Meng, Y., Zhu, M., 2019. Aeolian dust deposition and the perturbation of phosphorus transformations during long-term ecosystem development in a cool, semi-arid environment. Geochim. Cosmochim. Acta 246, 498–514.
- Gu, C., Dam, T., Hart, S.C., Turner, B.L., Chadwick, O.A., Berhe, A.A., Hu, Y., Zhu, M., 2020. Quantifying uncertainties in sequential chemical extraction of soil phosphorus using XANES spectroscopy. Environ. Sci. Technol. 54 (4), 2257–2267.
- Guo, B., Yang, H., Li, Y., 2011. The speciation of phosphorus in the sand particles in western Inner Mongolia, Mechanic Automation and Control Engineering (MACE). In: 2011 Second International Conference on. IEEE, pp. 2755–2757.
- Hammersley, A.P., Svensson, S.O., Hanfland, M., Fitch, A.N., Hausermann, D., 1996. Two-dimensional detector software: from real detector to idealised image or twotheta scan. High Pressure Res. 14 (4–6), 235–248.
- Harden, J.W., Taylor, E.M., Hill, C., Mark, R.K., McFadden, L.D., Reheis, M.C., Sowers, J. M., Wells, S.G., 1991. Rates of soil development from four soil chronosequences in the Southern Great Basin. Quat. Res. 35 (3), 383–399.
- Hedley, M.J., Stewart, J.W.B., Chauhan, B.S., 1982. Changes in inorganic and organic soil phosphorus fractions induced by cultivation practices and by laboratory incubations. Soil Sci. Soc. Am. J. 46 (5), 970–976.

Hoffmann, C., Funk, R., Wieland, R., Li, Y., Sommer, M., 2008. Effects of grazing and topography on dust flux and deposition in the Xilingele grassland, Inner Mongolia. J. Arid Environ. 72 (5), 792–807.

- Holmgren, G.G.S., 1967. A rapid citrate-dithionite extractable iron procedure. Soil Sci. Soc. Am. J. 31 (2), 210–211.
- Hooda, P., Rendell, A., Edwards, A., Withers, P., Aitken, M., Truesdale, V., 2000. Relating soil phosphorus indices to potential phosphorus release to water. J. Environ. Qual. 29 (4). 1166–1171.
- Huang, J., Yu, H., Guan, X., Wang, G., Guo, R., 2016. Accelerated dryland expansion under climate change. Nat. Clim. Chang. 6 (2), 166–171.
- Hudson-Edwards, K.A., Bristow, C.S., Cibin, G., Mason, G., Peacock, C.L., 2014. Solid-phase phosphorus speciation in Saharan Bodélé Depression dusts and source sediments. Chem. Geol. 384, 16–26.
- Johnson, A.H., Frizano, J., Vann, D.R., 2003. Biogeochemical implications of labile phosphorus in forest soils determined by the Hedley fractionation procedure. Oecologia 135 (4), 487–499.
- Kanayama, S., Yabuki, S., Yanagisawa, F., Motoyama, R., 2002. The chemical and strontium isotope composition of atmospheric aerosols over Japan: the contribution of long-range-transported Asian dust (Kosa). Atmos. Environ. 36 (33), 5159–5175.
- Kurtz, A.C., Derry, L.A., Chadwick, O.A., 2001. Accretion of Asian dust to Hawaiian soils: isotopic, elemental, and mineral mass balances. Geochim. Cosmochim. Acta 65 (12), 1971–1983
- Lang, F., Bauhus, J., Frossard, E., George, E., Kaiser, K., Kaupenjohann, M., Krüger, J., Matzner, E., Polle, A., Prietzel, J., Rennenberg, H., Wellbrock, N., 2016. Phosphorus in forest ecosystems: New insights from an ecosystem nutrition perspective. J. Plant Nutr. Soil Sci. 179 (2), 129–135.
- Lawrence, C.R., Reynolds, R.L., Ketterer, M.E., Neff, J.C., 2013. Aeolian controls of soil geochemistry and weathering fluxes in high-elevation ecosystems of the Rocky Mountains. Colorado. Geochim. Cosmochim. Acta 107, 27–46.
- Lee, S.-H., Baek, S.-H., Woo, S.I., Chung, C.-K., 2020. Estimation of in situ geotechnical properties on highly weathered granite using chemical weathering indices. Bull. Eng. Geol. Environ. 79, 3403–3415.
- Li, J., Zhang, G., Ruan, L., Yang, J., Wang, H., 2016. Sr–Nd elements and isotopes as tracers of dust input in a tropical soil chronosequence. Geoderma 262, 227–234.
- Li, W., Liu, X.-M., Chadwick, O.A., 2020. Lithium isotope behavior in Hawaiian regoliths: Soil-atmosphere-biosphere exchanges. Geochim. Cosmochim. Acta 285, 175–192.
- Liu, J., Yang, J., Liang, X., Zhao, Y., Cade-Menun, B.J., Hu, Y., 2014. Molecular Speciation of Phosphorus present in Readily Dispersible Colloids from Agricultural Soils. Soil Sci. Soc. Am. J. 78 (1), 47–53.
- Liu, W., Liu, C., Brantley, S.L., Xu, Z., Zhao, T., Liu, T., Yu, C., Xue, D., Zhao, Z., Cui, L., Zhang, Z., Fan, B., Gu, X., 2016. Deep weathering along a granite ridgeline in a subtropical climate. Chem. Geol. 427, 17–34.
- Longo, A.F., Ingall, E.D., Diaz, J.M., Oakes, M., King, L.E., Nenes, A., Mihalopoulos, N., Violaki, K., Avila, A., Benitez-Nelson, C.R., 2014. P-NEXFS analysis of aerosol phosphorus delivered to the Mediterranean Sea. Geophys. Res. Lett. 41 (11), 4043–4049.
- Ma, L.C., Liu, H.F., Wang, N., Li, H.Y., 2013. Forming reason of a continuous floating dust event in 2011 in Changchun. J. Meteorol. Environ. 29 (6), 24–30.
- Marx, S.K., Kamber, B.S., McGowan, H.A., Petherick, L.M., McTainsh, G.H., Stromsoe, N., Hooper, J.N., May, J.-H., 2018. Palaeo-dust records: a window to understanding past environments. Glob. Planet. Chang. 165, 13–43.
- Mokadem, F., Parkinson, I.J., Hathorne, E.C., Anand, P., Allen, J.T., Burton, K.W., 2015. High-precision radiogenic strontium isotope measurements of the modern and glacial ocean: Limits on glacial-interglacial variations in continental weathering. Earth Planet. Sci. Lett. 415, 111–120.
- Murphy, J., Riley, J.P., 1962. A modified single solution method for the determination of phosphate in natural waters. Anal. Chim. Acta 27, 31–36.
- Neff, J.C., Ballantyne, A.P., Farmer, G.L., Mahowald, N.M., Conroy, J.L., Landry, C.C., Overpeck, J.T., Painter, T.H., Lawrence, C.R., Reynolds, R.L., 2008. Increasing eolian dust deposition in the western United States linked to human activity. Nat. Geosci. 1 (3), 189–195.
- Nesbitt, H.W., 1979. Mobility and fractionation of rare earth elements during weathering of a granodiorite. Nature 279 (5710), 206–210.
- Okin, G.S., Mahowald, N., Chadwick, O.A., Artaxo, P., 2004. Impact of desert dust on the biogeochemistry of phosphorus in terrestrial ecosystems. Global Biogeochem. Cycl. 18 (2), GB2005.
- Pett-Ridge, J.C., 2009. Contributions of dust to phosphorus cycling in tropical forests of the Luquillo Mountains, Puerto Rico. Biogeochemistry 94 (1), 63–80.
- Pett-Ridge, J.C., Derry, L.A., Kurtz, A.C., 2009. Sr isotopes as a tracer of weathering processes and dust inputs in a tropical granitoid watershed, Luquillo Mountains, Puerto Rico. Geochim. Cosmochim. Acta 73 (1), 25–43.
- Porder, S., Hilley, G.E., Chadwick, O.A., 2007. Chemical weathering, mass loss, and dust inputs across a climate by time matrix in the Hawaiian Islands. Earth Planet. Sci. Lett. 258 (3), 414–427.
- Prăvălie, R., 2016. Drylands extent and environmental issues. A global approach. Earth Sci. Rev. 161, 259–278.
- Rao, W., Yang, J., Chen, J., Li, G., 2006. Sr-Nd isotope geochemistry of eolian dust of the arid-semiarid areas in China: implications for loess provenance and monsoon evolution. Chin. Sci. Bull. 51 (12), 1401–1412.
- Rasmussen, C., McGuire, L., Dhakal, P., Pelletier, J.D., 2017. Coevolution of soil and topography across a semiarid cinder cone chronosequence. Catena 156, 338–352.
- Ravel, B., Newville, M., 2005. ATHENA, ARTEMIS, HEPHAESTUS: data analysis for X-ray absorption spectroscopy using IFEFFIT. J. Synchrotron Radiat. 12 (4), 537–541.
- Rea, P., Ma, L., Gill, T.E., Gardea-Torresdey, J., Tamez, C., Jin, L., 2020. Tracing gypsiferous White Sands aerosols in the shallow critical zone in the northern

- Sacramento Mountains, New Mexico using Sr/Ca and 87Sr/86Sr ratios. Geoderma 372. 114387.
- Richardson, S.J., Peltzer, D.A., Allen, R.B., McGlone, M.S., Parfitt, R.L., 2004. Rapid development of phosphorus limitation in temperate rainforest along the Franz Josef soil chronosequence. Oecologia 139 (2), 267–276.
- Robertson, G.P., Coleman, D.C., Bledsoe, C.S., Sollins, P., 1999. Standard Soil Methods for Long-Term Ecological Research. Oxford University Press, New York.
- Sauchyn, D., Barrow, E., Hopkinson, R., Leavitt, P., 2002. Aridity on the Canadian Plains. Géogr. Phys. Quat 56 (2–3), 247–259.
- Schwertmann, U., 1964. Differentiation of soil iron oxides by extraction with ammonium oxalate-solution. Z. Pflanzenernähr. Düng. Bodenkd. 105, 194–202.
- Selmants, P.C., Hart, S.C., 2008. Substrate age and tree islands influence carbon and nitrogen dynamics across a retrogressive semiarid chronosequence. Global Biogeochem. Cycl. 22 (1), GB1021.
- Shao, Y., Dong, C.H., 2006. A review on East Asian dust storm climate, modelling and monitoring. Glob. Planet. Chang. 52 (1), 1–22.
- Shen, Z.X., Cao, J.J., Arimoto, R., Zhang, R.J., Jie, D.M., Liu, S.X., Zhu, C.S., 2007. Chemical composition and source characterization of spring aerosol over Horqin sand land in northeastern China. J. Geophys. Res. 112, D14315.
- Sims, J.T., 2000. Soil test phosphorus: Olsen P. In: Pierzynski, G.M. (Ed.), Methods of Phosphorus Analysis for Soils, Sediments, Residuals, and Waters. Southern Cooperative Series Bulletin, Kansas, US, pp. 20–21.
- Soil Survey Staff., 2014. Keys to Soil Taxonomy, 12th ed. United States Department of Agriculture, Natural Resources Conservation Service, Washington, DC.
- Stemmer, M., Gerzabek, M.H., Kandeler, E., 1998. Organic matter and enzyme activity in particle-size fractions of soils obtained after low-energy sonication. Soil Biol. Biochem. 30 (1), 9–17.
- Sun, J., 2002. Provenance of loess material and formation of loess deposits on the Chinese Loess Plateau. Earth Planet. Sci. Lett. 203 (3), 845–859.
- Sun, J., Ding, Z., Liu, T., 1998. Desert distributions during the glacial maximum and climatic optimum: example of China. Episodes-Newsmagaz. Int. Union Geol. Sci. 21 (1), 28–31.
- Tiessen, H., Moir, J.O., 1993. Characterization of available phosphorus by sequential extraction. In: Carter, M.R. (Ed.), Soil Sampling and Methods of Analysis. Lewis, Chelsea, MI, pp. 75–86.
- Tyrrell, T., 1999. The relative influences of nitrogen and phosphorus on oceanic primary production. Nature 400 (6744), 525–531.

- Vincent, A.G., Turner, B.L., Tanner, E.V.J., 2010. Soil organic phosphorus dynamics following perturbation of litter cycling in a tropical moist forest. Eur. J. Soil Sci. 61 (1), 48–57.
- Vogel, C., Helfenstein, J., Massey, M.S., Sekine, R., Kretzschmar, R., Beiping, L., Peter, T., Chadwick, O.A., Tamburini, F., Rivard, C., Herzel, H., Adam, C., Pradas del Real, A. E., Castillo-Michel, H., Zuin, L., Wang, D., Félix, R., Lassalle-Kaiser, B., Frossard, E., 2021. Microspectroscopy reveals dust-derived apatite grains in acidic, highlyweathered Hawaiian soils. Geoderma 381, 114681.
- Vogel, D., 1975. Precambrian weathering in acid metavolcanic rocks from the Superior Province, Villebon Township, South-central Quebec. Can. J. Earth Sci. 12 (12), 2080–2085.
- Weis, D., Kieffer, B., Maerschalk, C., Barling, J., de Jong, J., Williams, G.A., Hanano, D., Pretorius, W., Mattielli, N., Scoates, J.S., Goolaerts, A., Friedman, R.M., Mahoney, J. B., 2006. High-precision isotopic characterization of USGS reference materials by TIMS and MC-ICP-MS. Geochem. Geophys. Geosyst. 7, Q08006.
- Xie, Y., Chi, Y., 2016. Geochemical investigation of dry- and wet-deposited dust during the same dust-storm event in Harbin, China: constraint on provenance and implications for formation of aeolian loess. J. Asian Earth Sci. 120, 43–61.
- Xie, Y., Chi, Y., Meng, J., Guo, L., Wang, Y., 2015. Grain-size and Sr-Nd isotopic compositions of dry- and wet-deposited dusts during the same dust-storm event in Harbin, China: implications for source, transport-deposition modes, dynamic mechanism and formation of eolian loess. Environ. Earth Sci. 74 (8), 6489-6502.
- Xie, Y., Yuan, F., Zhan, T., Kang, C., Chi, Y., 2018a. Geochemical and isotopic characteristics of sediments for the Hulun Buir Sandy Land, Northeast China: implication for weathering, recycling and dust provenance. Catena 160, 170–184.
- Xie, Y., Yuan, F., Zhan, T., Kang, C., Chi, Y., Ma, Y., 2018b. Geochemistry of loess deposits in northeastern China: constraint on provenance and implication for disappearance of the large Songliao palaeolake. J. Geol. Soc. 175, 146–162.
- Yu, H., Chin, M., Yuan, T., Bian, H., Remer, L.A., Prospero, J.M., Omar, A., Winker, D., Yang, Y., Zhang, Y., Zhang, Z., Zhao, C., 2015. The fertilizing role of African dust in the Amazon rainforest: a first multiyear assessment based on data from Cloud-Aerosol Lidar and infrared Pathfinder Satellite Observations. Geophys. Res. Lett. 42 (6), 1094, 1001.
- Zhang, Z., Goldstein, H.L., Reynolds, R.L., Hu, Y., Wang, X., Zhu, M., 2018. Phosphorus speciation and solubility in aeolian dust deposited in the interior American West. Environ. Sci. Technol. 52 (5), 2658–2667.
- Zhang, Z., Zhao, Z., Liu, C., Chadwick, O.A., Liang, C., Hu, Y., Vaughan, K.L., Zhu, M., 2021. Vertical patterns of phosphorus concentration and speciation in three forest soil profiles of contrasting climate. Geochim. Cosmochim. Acta 310, 1–18.